Volume 1 | Number 1 | Jan 2013 | Pages 1–100

Dalton Transactions

An international journal of inorganic chemistry
www.rsc.org/dalton

ROYAL SOCIETY OF CHEMISTRY

ROYAL SOCIETY OF CHEMISTRY

www.rsc.org/dalton

New approach in the synthesis of $La_{1-x}Gd_xFeO_3$ perovskite nanoparticles - structural and magnetic characterization

R.J. Wiglusz[*,1,2], K. Kordek[1], M. Małecka[1], A. Ciupa[1], M. Ptak[1], R. Pazik[1,2], P. Pohl[3], D. Kaczorowski[1,2]

[1]*Institute of Low Temperature and Structure Research, PAS, Okolna 2, 50-422 Wroclaw, Poland*

[2]*Centre for Advanced Materials and Smart Structures, Polish Academy of Sciences, Okolna 2, 50-950 Wroclaw, Poland*

[3]*Wroclaw University of Technology, Chemistry Department, Analytical Chemistry Division, Wybrzeze Wyspianskiego 27, 50-370 Wroclaw, Poland*

Abstract

Series of the high crystalline orthoferrite nanoparticles (type $La_{1-x}Gd_xFeO_3$, where x = from 0 to 1) were prepared using the self-combustion method. Extensive studies including X-ray diffraction, Rietveld refinement and Fourier transform infrared spectroscopy as well as Raman spectroscopy confirmed the orthorhombic space group *Pnma* of the obtained materials. The calculated average grain size for powders is in the range of 30 to 80 nm. Magnetic characterization of the $La_{1-x}Gd_xFeO_3$ series, performed at 1.72 K, indicated an antiferromagnetic state characterized by some canting of iron magnetic moments, in good agreement with the data reported for similar fine-particle systems.

Keywords: Perovskite ferrites, Nanoparticle, Self-combustion synthesis, Magnetic behavior

[*]Corresponding author:

R.Wiglusz@int.pan.wroc.pl

Phone: +48-71-3954-159,

Fax: +48-71-344-10-29

1. Introduction

A large number of inorganic oxide compounds adopt a perovskite structure with a general formula ABO_3. Perovskite structure is built up of the corner sharing BO_6 octahedra with the A ions located in the 12-fold cavities. The ideal perovskite structure belongs to the *Pm3m* space group. It is well known that three different distortions can occur in the perovskite architecture: (i) tilting, (ii) distortion of the BO_6 octahedra and (iii) displacements of the B cations within the polyhedra. The $LaFeO_3$ and $GdFeO_3$ are perovskite materials that crystallize in the orthorhombic space group *Pnma* showing a distorted perovskite-type structure as a result of the FeO_6 octahedra tilting[1]. The tilt angle α increases with a decrease of the atomic number of the rare earth elements meaning that the structure becomes less distorted.

Lanthanum and gadolinium orthoferrites have received a lot of attention due to their potential applications in fuel cells[2] and catalysis[3,4]. They are also of interest as magnetic materials and oxygen sensors due to their mixed electronic and ionic conductivity with a nonlinear response to the applied oxygen pressure[5,6,7,8,9,10,11]. It was also reported that nanosized orthoferrites can be used as photo catalysts in the decomposition of water or the degradation of dyes under the light irradiation[12,13]. However, mechanisms of those processes are still poorly understood. Owing to the fact that the properties of nano-orthoferrites are related to their surface area and homogeneity, different methods of synthesis were investigated, including sol-gel[14], hydrothermal[15], combustion[16,17] and sonochemical methods[18]. Most importantly, the majority of synthetic techniques require a high annealing temperature, which results in a poor homogeneity, a high porosity as well as a large distribution of the particle size of the resulting nanostructures.

It is worth noting that $LaFeO_3$ and $GdFeO_3$ exhibit non-trivial magnetic properties. The two orthoferrites order antiferromagnetically with small ferromagnetic components. The magnetic moments of Fe^{3+} ions are aligned antiferromagnetically along *a*-axis with a small Dzyaloshinskii-Moriya interaction[19,20]. Interestingly, $LaFeO_3$ possesses the highest Neel temperature (738 K) among all known orthoferrites[19].

This work is focused on the self-combustion synthesis of the nanocrystalline perovskite $La_{1-x}Gd_xFeO_3$ particles with a broad concentration range of Gd^{3+} ions used as a dopant. Our particular interest is put on the characterization of structural and magnetic properties of given compounds with a strong emphasis on the role of Gd^{3+} ions on the modulation of the structure and magnetic response.

2. Experimental

2.1. Apparatus

The crystal structure of the $La_{1-x}Gd_xFeO_3$ was examined by means of the XRD technique by collecting patterns in the 2Θ range of 5–120° with a X'Pert PRO X-ray diffractometer (Cu, Kα1: 1.54060 Å) (PANalytical). The microstructure and the morphology of nanoparticles were studied using high resolution transmission electron microscopy (HRTEM) with a Philips CM-20 Super Twin microscope operated at 200 kV. Samples for measurements were prepared by taking a droplet of the ethanol/water suspension of nanoparticles and their deposition on a copper microscope grid covered with perforated carbon. The primary size of particles was evaluated using the volume weighted formula:

$$d_{av} = \frac{\sum n_i d_i^4}{\sum n_i d_i^3}, (1)$$

where d_{av} is the average particle size, n – the number of particles and d represents the particle diameter. The elemental analysis was carried out using a scanning electron microscope FEI Nova NanoSEM 230 equipped with an EDS spectrometer (EDAX PegasusXM4). Up to 10 measurements were made from different random areas for each sample. Polycrystalline infrared spectra were recorded with a Bio-Rad 575C FT-IR spectrometer in a KBr pellet for the 1200–400 cm^{-1} region and in a Nujol suspension for the 500–100 cm^{-1} region. Raman measurements were carried out with a Micro-Raman system Renishaw inVia equipped with a Leica DM 2500 M microscope and a CCD camera for the detection. A 830 nm diode laser was used as the excitation source. Magnetization measurements were performed at 1.72 K in magnetic fields up to 5T using a Quantum Design MPMS-5 SQUID magnetometer.In addition, the elemental analysis of $La_{1-x}Gd_xFeO_3$ nanoparticles, i.e., $GdFeO_3$, $LaFeO_3$ and $La_{0.5}Gd_{0.5}FeO_3$, was made by inductively coupled plasma optical emission spectrometry (ICP OES) using an Agilent 720 instrument. The spectrometer used was equipped with a high-resolution echelle-type polychromator and a VistaChip II CCD detector. The plasma was operated in a standard quartz torch with an injector tube of 2.4 mm ID; a single-pass glass cyclonic spray chamber and an OneNeb pneumatic concentric nebulizer were used to introduce solutions of samples and standards by the pneumatic nebulization. Operating conditions recommended by the manufacturer for solutions with a high level of dissolved-solids were applied. Samples (50.0 mg) of synthesized and isolated nanoparticles were digested in freshly prepared *aqua regia* (2.0 ml) by heating them at 85-90°C for 0.5 h using a temperature-controlled DigiPREP block digestion system (SCP Science). Sample aliquots

obtained were diluted with deionized water to 100 ml. The concentration of Fe, Gd and La in resulting sample solutions were determined by ICP OES against simple standard solutions (ranged within 0.1-2 $\mu g \cdot ml^{-1}$) after adequate dilutions. The whole analysis was repeated 3 times (n=3), final results were expressed in $\mu g \cdot g^{-1}$, considering the mass of samples, the volume of sample solutions and the dilution factor.

2.2. Synthesis of $La_{1-x}Gd_xFeO_3$ nanoparticles

All of the $La_{1-x}Gd_xFeO_3$ nanoparticles were prepared by the self-combustion method. A typical preparation procedure, for instance for the $La_{0.5}Gd_{0.5}FeO_3$ nanoparticles, involved the usage of the following substrates 0.326 g (1 mmol) of La_2O_3 (99.9% Alfa Aesar), 0.3625 g (1 mmol) of Gd_2O_3 (99.9% Alfa Aesar), 1.616 g (4 mmol) of $Fe(NO_3)_3 \cdot 9H_2O$ (99.9% Alfa Aesar) and 0.93 g (12.4 mmol) of H_2NCH_2COOH (99% Alfa Aesar). All oxides were digested in an excess of the HNO_3 (ultra-anal Avantor Performance Materials) and re-crystallized three times. Afterwards, La^{3+}, Gd^{3+} nitrates were dissolved in deionized water and $Fe(NO_3)_3 \cdot 9H_2O$ along with glycine as a fuel were added. Final solution was stirred at 80°C, dried at 120°C and finally transferred into a preheated electric furnace at 500°C. Once the auto-combustion started, the front spontaneously propagated and converted the dried gel into the brown final product in form of fine powder.

3. Results and Discussion

3.1. Structure evolution

The characterization of the $La_{1-x}Gd_xFeO_3$ structural properties was done by the XRD technique as a function of a broad Gd^{3+} concentration. As it can be seen in Figure 1, for the whole concentration range of Gd^{3+} ions only pure crystalline phases, corresponding to the reference standards of the $LaFeO_3$ (ICSD 371493)[21] and $GdFeO_3$ (ICSD 470067)[22], are present. The structure of the $La_{1-x}Gd_xFeO_3$ can be described by the pseudo-cubic modification ascribed to the *Pnma* space group characteristic of the orthoferrite family. Unit cell parameters for selected samples were calculated by the Rietveld method[23] with the anisotropic approach[24] using Maud 2.50 software[25]. The projection of the unit cell with the indication of the coordination polyhedra are presented in Figure 2 whereas results of all calculations are given in tables I and II.
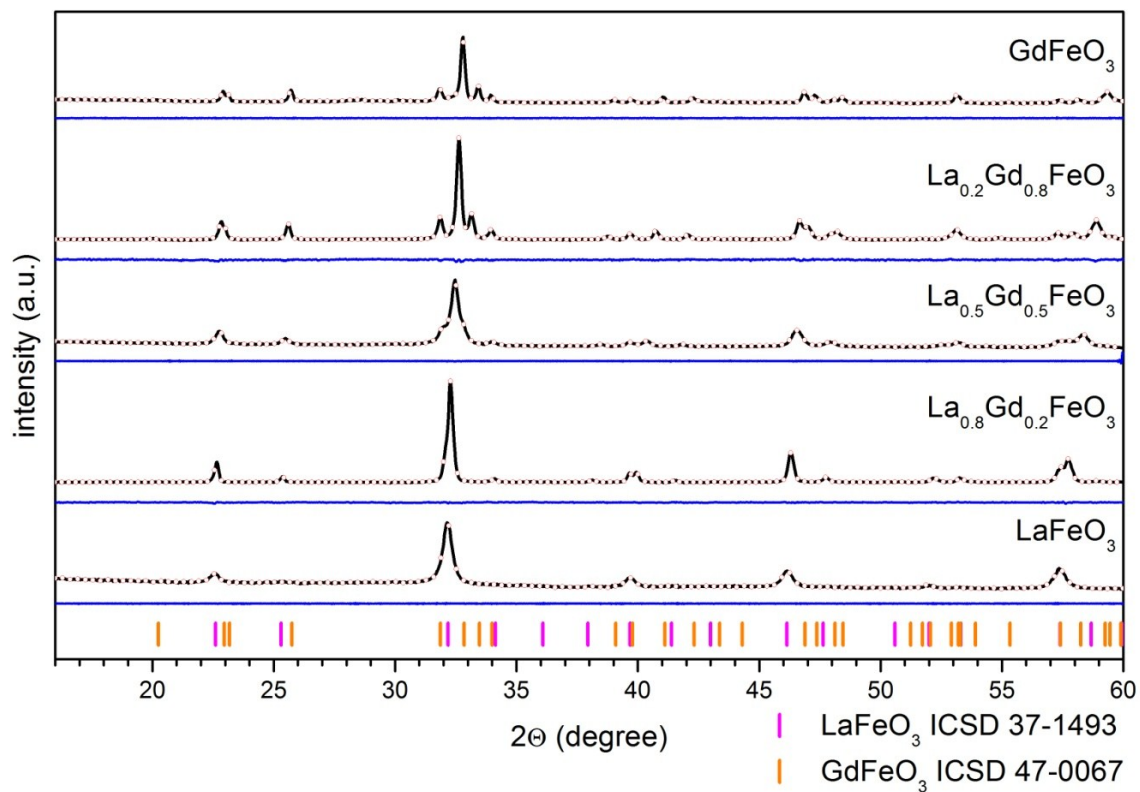
Figure 1. XRD patterns of the $La_{1-x}Gd_xFeO_3$ as a function of the Gd^{3+} content.
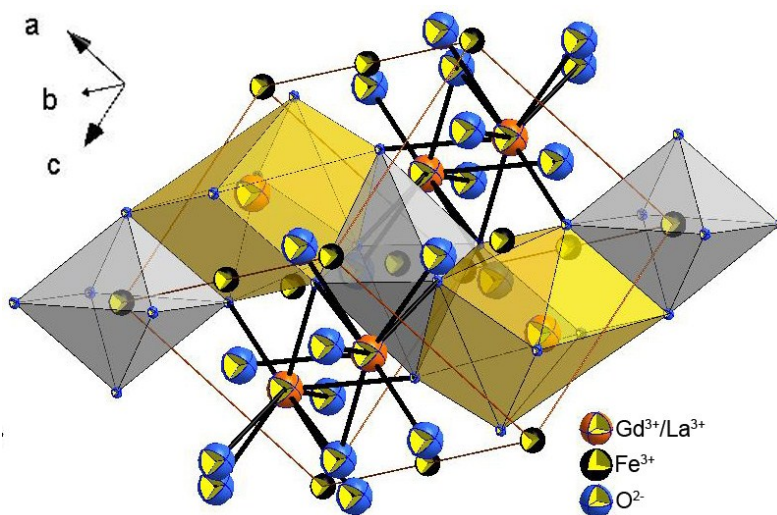

Figure 2. The projection of the orthoferrite $La_{0.5}Gd_{0.5}FeO_3$ unit cell with the indication of the coordination polyhedra.

Table I. Cell parameters of the $La_{1-x}Gd_xFeO_3$ nanoparticles based on the Rietveld refinement.

Sample	a (Å)	b (Å)	c (Å)	V (Å³)	grain size (nm)	R_w (%)
single crystal[26]	5.6160	7.6680	5.3460	230.22	-	-
LaFeO₃	5.5595(0)	7.8703(0)	5.5589(9)	243.22(9)	29	1.26
La₀.₈Gd₀.₂FeO₃	5.5750(0)	7.8290(6)	5.5180(4)	240.84(2)	35	1.21
La₀.₅Gd₀.₅FeO₃	5.5936(1)	7.7763(2)	5.4540(2)	237.06(1)	39	1.02
La₀.₂Gd₀.₈FeO₃	5.6105(9)	7.7253(3)	5.3989(2)	234.00(3)	73	0.92
GdFeO₃	5.6148(2)	7.6837(6)	5.3555(2)	231.14(9)	75	1.62

The results suggested successful incorporation of Fe^{3+} at the La^{3+}, and Gd^{3+} cation sites confirming the formation of the orthorhombic phase of $LaFeO_3$, $La_{1-x}Gd_xFeO_3$ and $GdFeO_3$. A good agreement with those for standards was found. The observed difference in the unit cell volume, *V*, agrees with that expected from the difference in size volume of the involved rare-earth ions. The progressive decrease of the cell volume as well as *b* and *c* parameters upon the Gd^{3+} doping were found due to the substitution of a large La^{3+} (C.N. 8 - 1.160 Å) by smaller Gd^{3+} (C.N. 8 - 1.053 Å) resulting in contraction of the unit cell. It was found that the Fe-O2 bond length are more affected and shortened with the increase of the concentration of Gd^{3+} ions whereas Fe-O1 bonds remain almost the same. In a consequence, the bond angle Fe-O2-Fe increases with the Gd^{3+} concentration. This leads to the increase of the tilting of the Fe-O octahedral geometry and the higher orthorhombic distortion in case of Gd^{3+} doping[27].

Table II. Atomic parameters of a representative sample of $La_{0.5}Gd_{0.5}FeO_3$ nanoparticles.

Sample		$La_{0.5}Gd_{0.5}FeO_3$, Z=4				
Space group		Orthorhombic *Pnma* (62)				
Calculated cell parameters		a = 5.5936(1) Å b = 7.7763(2) Å c = 5.4540(2) Å V = 237.24(1)Å³				
R_w		1.02%				
R_{wnb}		0.93%				
R_{all}		0.79%				
R_{nb}		0.80%				
σ		0.94%				
Selected contacts						
Gd|La – La|Gd		3.8398(1) Å				
Gd|La – O		2.5165(0) Å				
Fe – Fe		3.9062(1) Å				
Fe – O		2.2464(0) Å				
O – Fe – O		84.20(0) °				
Atom	Wyckoff positions	x	y	z	B_{iso}	Occ. (<1)
Gd1	4c	0.04560	0.25	0.49120	0.0527	0.5
Fe1	4a	0	0	0	0.0448	
O1	4c	0.47830	0.25	0.61750	0.0362	
O2	8d	0.30940	0.04220	0.25560	0.0115	
La1	4c	0.04560	0.25	0.49120	0.0213	0.5

3.2. Infrared and Raman spectroscopy

The GdFeO$_3$ and LaFeO$_3$ orthoferrites crystallize in the *Pbnm* (D_{2h}^{16}, No. 62, *Z*=4) orthorhombic space group. The factor group analysis shows that the Brillouin zone center normal modes are distributed among $7A_g + 8A_u + 5B_{1g} + 10B_{1u} + 7B_{2g} + 8B_{2u} + 5B_{3g} + 10B_{3u}$ irreducible representations. A_g, B_{1g}, B_{2g}, and B_{3g} modes are Raman active ($7A_g + 5B_{1g} + 7B_{2g} + 5B_{3g}$) whereas B_{1u}, B_{2u} and B_{3u} modes are IR active ($9B_{1u} + 7B_{2u} + 9B_{3u}$ optical phonons and three $B_{1u} + B_{2u} + B_{3u}$ acoustic phonons). Remaining A_u modes are silent, therefore the group theory predicts 24 Raman and 25 IR active modes.
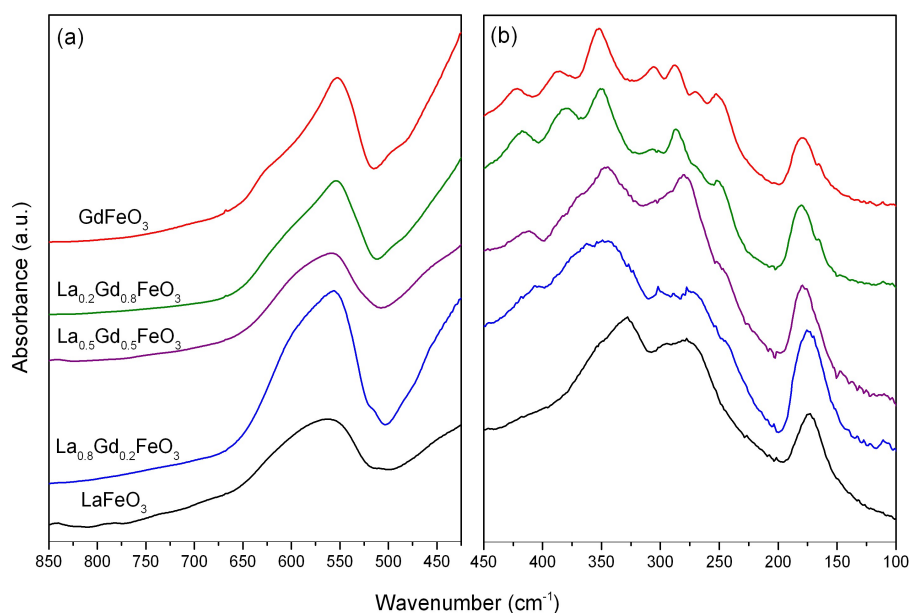

Figure 3. The comparison of IR spectra for La$_{1-x}$Gd$_x$FeO$_3$ as a function of the Gd^{3+} content in mid-IR (a) and far-IR (b) ranges.

Figure 3a and 3b presents room temperature IR spectra of synthesized solid solutions. The disagreement in the number of bands with the group theory prediction can be explained by the fact that some bands are located very close to each other and hence cannot be separated due to their overlap. The lattice dynamic calculations performed for the isostructural orthoferrite, NdFeO$_3$, confirmed overlapping of some IR and Raman bands[28]. These calculations as well as other literature data show that modes above 490 cm^{-1} can be assigned mainly to the stretching vibrations of Fe-O bonds while bands in the $500 - 250$ cm^{-1} region to the bending Fe-O vibrations. Most of bands below 200 cm^{-1} have the strongest contribution coming from translational motions of the La^{3+}/Gd^{3+} ions[27,28].

The spectrum of the GdFeO$_3$ sample presents 12 vibrational modes at 625, 552, 496, 422, 387, 352, 306, 287, 270, 252, 179 and 166 cm^{-1}. As it can be seen, the increasing concentration of the La^{3+} ions causes a progressive evolution of the IR spectra. First, the

width of the observed bands increases significantly. This observations is in accordance with the XRD analysis. The samples doped with high concentrations of La^{3+} are forming small particles meaning that the addition of the Gd^{3+} favors crystallization of bigger crystallites. It is well known that when the particle size decreases, phonon properties are significantly affected due to a few factors, i.e., distribution of the crystallite size, creation of defects, phonon confinement effect, strains and etc[29]. We think that the band broadening is strong for $La_xGd_{1-x}FeO_3$ solid solutions due to an additional contribution coming from the substitutional disorder and/or a possible presence of amorphous phases. The elemental composition of perovskite-type structures is very often non stoichiometric due to oxygen vacancies, which also can result in band broadening[30]. Secondly, all IR bands are visibly shifted towards lower wavenumbers. Moreover, these changes are proportional to the concentration of dopant ions. For instance, the intense band at 387 cm^{-1} for $GdFeO_3$ shifts progressively to 382, 370, 364 and 354 cm^{-1} for samples containing 20, 50, 80 and 100 % of La^{3+} ions, respectively. The increasing concentration of La^{3+} ions causes expansion of the unit cell, since the substitution of Gd^{3+} by La^{3+} ions with higher ionic radii causes a stronger tilting of the FeO_6 units. The increase of the unit cell slightly decreases the force constants of vibrating bonds, thereby IR absorption bands are downshifted[31]. Lastly, the intensity of some IR bands decreases with the increasing concentration of La^{3+} ions. For instance, bands at 387, 270, 306 and 165 cm^{-1} observed for $GdFeO_3$ disappear already for the $La_{0.5}Gd_{0.5}FeO_3$ sample. This behavior can be attributed to the progressive structural orthorhombic distortion induced by the substitution, the shape of crystallites, their distribution, as well as the preferential orientation and/or creation of defects.

In order to get more information regarding the local structure, the Micro-Raman spectra were recorded at room temperature for the $La_{1-x}Gd_xFeO_3$ (where x − 1, 0.5 and 0) perovskite series (Figure 4). The Micro-Raman spectroscopy in crystals is due to the scattering of light by the lattice vibrations, leading to the annihilation or the creation of crystal phonons. As it was mentioned earlier, the $La_{1-x}Gd_xFeO_3$ compounds have the orthorhombic structure and the energy bands for the compounds are shown up to 600 cm^{-1}, labeled according to the A_g and B_{2g} symmetry of the *Pnma* space group. Thus, according to the analysis presented by I.S. Smirnova[32], there are the B_{1u}, B_{2u}, B_{3u} as well as A_u modes, which remain silent. In general, the Raman modes are classified into 12 internal and 9 external modes. Five out of 12 internal modes are described as the stretching type [$A_g(1)$, $A_g(2)$, $B_{3g}(2)$, $B_{2g}(1)$, and 6 $B_{2g}(2)$]. The remaining 7 internal modes are classified as the bending type ($A_g(3)$, $A_g(4)$, $A_g(7)$, $B_{1g}(2)$, $B_{3g}(1)$, $B_{2g}(3)$, and $B_{2g}(7)$]. Six external modes are ascribed as the translational type [$A_g(5)$,

$A_g(6)$, $B_{3g}(4)$, $B_{3g}(5)$, $B_{2g}(5)$, and $B_{2g}(6)$] and 3 as the rotational type [$B_{1g}(1)$, $B_{3g}(3)$, and $B_{2g}(4)$]. In case of $La_{1-x}Gd_xFeO_3$, all observed modes are positioned below 200 cm^{-1} for the La^{3+} and Gd^{3+} vibrations. Oxygen octahedral tilt modes can be found between 200 and 300 cm^{-1} for La3+, whereas for Gd^{3+} doping the range is a bit brooder and covers 200 - 400 cm^{-1}. The modes between 400 cm^{-1} and 450 cm^{-1} are the oxygen octahedral bending vibrations while modes above 500 cm^{-1} are ascribed to the oxygen stretching vibrations[27,33]. All bands visible below 300 cm^{-1} in La^{3+} compounds are shifted towards higher energies with respect to Gd^{3+} ones. The differences between spectra are associated with the dissimilar distortions caused by La^{3+} and Gd^{3+} contents.
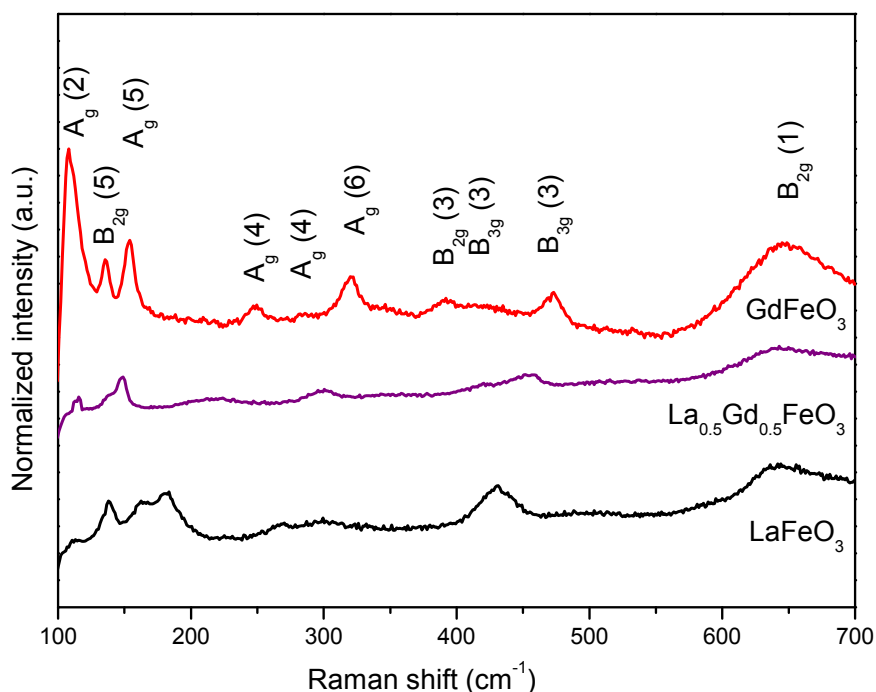

Figure 4. The comparison of the Micro-Raman spectra at frequencies below 700 cm^{-1} for $La_{1-x}Gd_xFeO_3$ perovskite nanoparticles.

3.3. Morphological analysis

The particle size and the morphology of the $La_{1-x}Gd_xFeO_3$ nanoparticles was estimated using the high resolution TEM technique. Representative TEM and SAED images are shown in Figure 5.
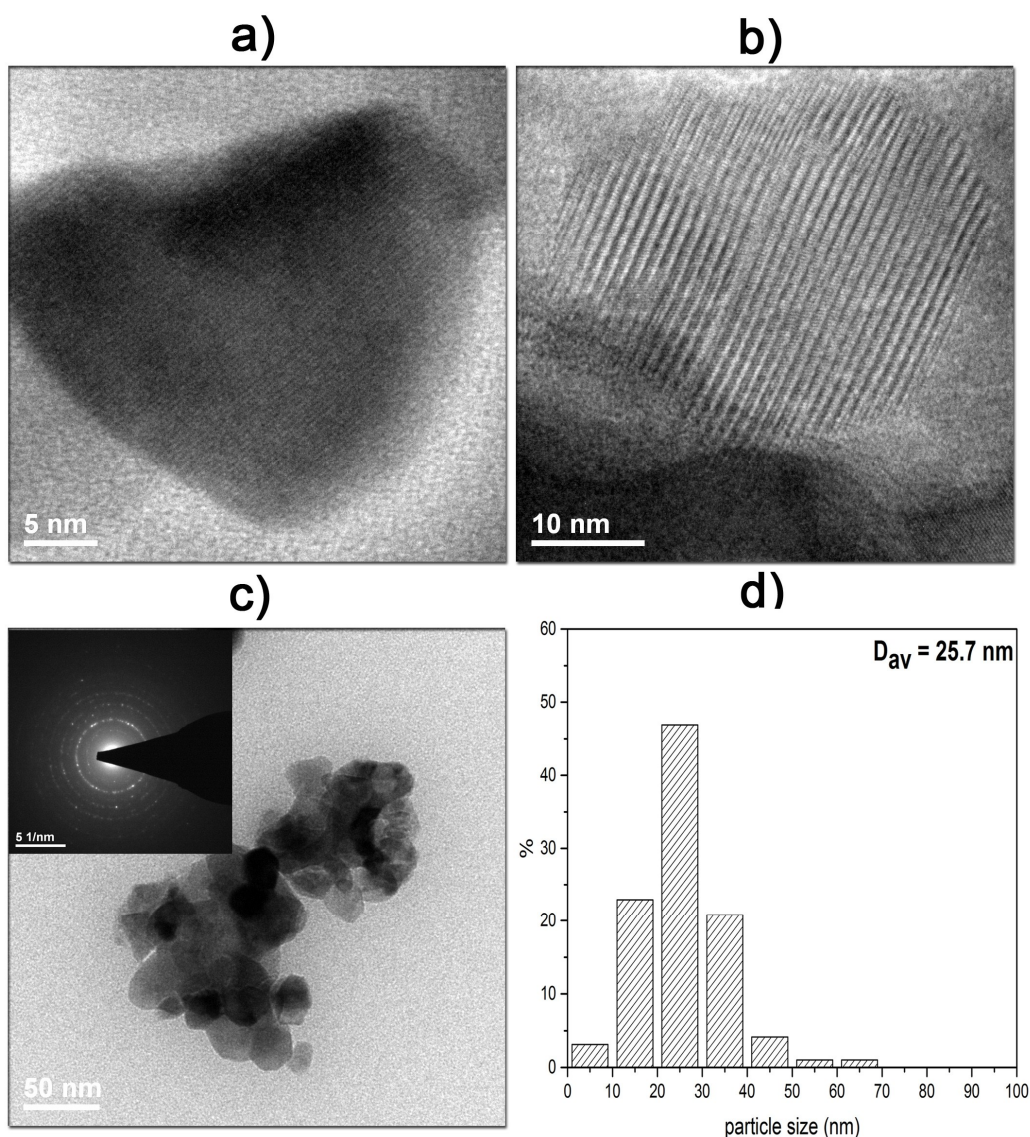
Figure 5. TEM (a, b, c), SAED (c inset) images as well as particle size distribution of the $La_{0.5}Gd_{0.5}FeO_3$ nanoparticles.

As it can be seen, the particles are forming fairly large agglomerates with rather irregular shapes. In fact, the formation of such objects is typical for the combustion synthesis, which promotes the agglomeration process. It disclosed aggregates of nanoparticles with irregular shape and quite uniform size of approximately 30–40 nm in diameter and about 50–60 nm in length (see Figure 6. – an inset). SAED images showed the appearance of well-developed and spotty rings with positions and distances close to the reference standards. The average particle size of all samples is around 30-80 nm. The content of the La^{3+} and Gd^{3+} ions was checked using the SEM-EDS technique (Figure 6). The results are satisfactory and show a good agreement with the assumed quantity of both cations in the orthoferrite structure.
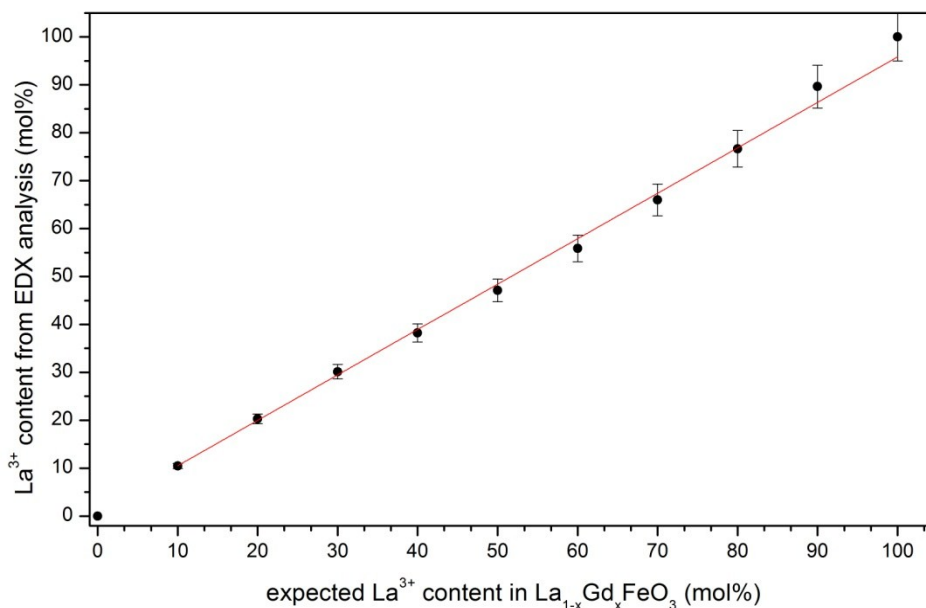
Figure 6. The content of the La^{3+} in the $La_{1-x}Gd_xFeO_3$ nanoparticles.

3.4. Magnetic properties

In order to further characterize the synthesized $La_{1-x}Gd_xFeO_3$ nanoparticles, their magnetic properties were determined by measuring the field dependencies of the magnetization at 1.72 K. The results have been gathered in Figure 7. The $\sigma(B)$ data obtained for $LaFeO_3$ (see Figure 7a) is fully consistent with a canted antiferromagnetic ordering of the Fe^{3+} spin, reported in the literature[19,20,34]. The magnetization does not show any tendency towards saturation up to the terminal field of 5 T. The value measured in this field is 6.1(3) emu/g that corresponds to the magnetic moment of only 0.27(1) μ_B, being just small fraction of the ordered magnetic moment $m_s = 5.92$ μ_B calculated for a free Fe^{3+} ion with $^6S_{5/2}$ ground multiplet. A small hysteresis in $\sigma(B)$ brings about a remanence of 1.1(4) emu/g [1.1(2) μ_B] that should be attributed to a ferromagnetic component in the magnetic structure of $LaFeO_3$ arising due to the Dzyaloshynskii-Moriya interactions[19,20]. Remarkably, almost the same remanence was found for $GaFeO_3$. In this case, however, the canting effect is not directly visible in the $\sigma(B)$ data because the measured magnetization is dominated by a large paramagnetic contribution due to Gd^{3+} ions. In 5 T, the magnetization reaches a value of 123(8) em/g that is about 20 times larger than that in the La-bearing counterpart (see the bottom panel in Figure 7b). Assuming that the Fe^{3+} component achieves in 5T a magnitude similar to that in $LaFeO_3$, the magnetization due to the rare-earth sublattice can be estimated to be about 117 μ_B. This value implies the magnetic moment of 5.5 μ_B that is distinctly smaller than the theoretical free Gd^{3+}

ion value of $7\,\mu_B$. This finding is in concert with the paramagnetic character of the Gd sublattice of $GaFeO_3$ at 1.72 K[35].
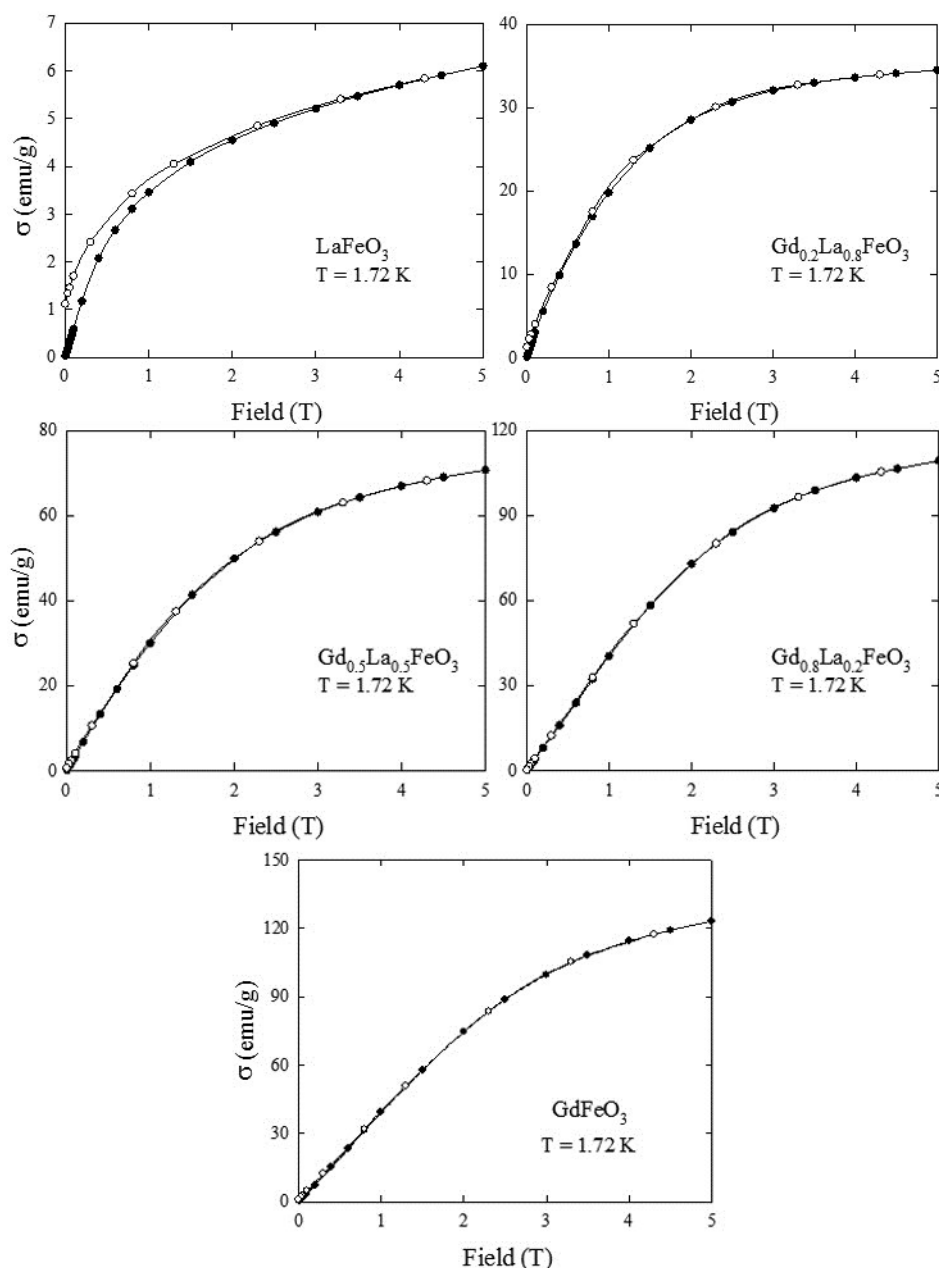

Figure 7. Magnetic field variation of the magnetization in the $La_{1-x}Gd_xFeO_3$ samples taken at 1.72 K with increasing (full symbols) and decreasing (open symbols) magnetic field strength. Prior to each measurement, the specimen was cooled to the target temperature in zero field.

The overall shapes of the $\sigma(B)$ curves measured for the solid solutions $La_{1-x}Gd_xFeO_3$ are similar to those of the terminal phases. Assuming the contributions due to the Fe^{3+} and Gd^{3+} ions equal to those estimated for $LaFeO_3$ and $GaFeO_3$, one may calculate the expected magnitude of the magnetization at 1.72 K and in 5 T to be 30, 65, and 100 emu/g for $La_{0.8}Gd_{0.2}FeO_3$, $La_{0.5}Gd_{0.5}FeO_3$, and $La_{0.2}Gd_{0.8}FeO_3$, respectively. As can be inferred from

inspecting the panels in Figure 7, all three values are reasonably close to the experimental results [34(5), 70(7), and 109(9) emu/g, respectively]. The performed analysis of the magnetic data of $La_{1-x}Gd_xFeO_3$ can be thus considered as another verification of the chemical composition of the investigated nanopowders derived from the XRD and SEM-EDS studies.

4. Conclusions

The series of highly crystalline orthoferrite nanoparticles $La_{1-x}Gd_xFeO_3$ with x ranging from 0 to 1 were prepared using self-combustion method that allows low-cost and fast synthesis of these perovskites. The prepared materials crystallize in the orthorhombic space group *Pnma* as a pure matrix. The lattice parameters and the unit cell volume monotonically decrease with increasing Gd^{3+} content, which can be attributed to a change in the A-site ionic radius. The characterization with infrared and Micro-Raman spectroscopy confirmed a pure phase nature of the prepared $La_{1-x}Gd_xFeO_3$ series. The average particle size, calculated using the Rietveld method, was found to span from 30 to 80 nm. Similar result was obtained from the TEM observations.

The magnetization measurements at 1.72 K revealed for all the investigated samples a canted antiferromagnetic ordering of the magnetic moments carried on trivalent iron ions. The contribution due to Gd^{3+} ions was found purely paramagnetic. Possibly, the gadolinium moments order magnetically at lower temperatures. Further comprehensive magnetic studies at elevated temperatures (the Neel points in the $La_{1-x}Gd_xFeO_3$ series are expected to be close to 738 K reported for the terminal $LaFeO_3$ phase[19]) are compulsory in order to examine prospective of using these materials in practical applications.

5. Acknowledgements

6. References

[1] N. J. R. Hayes, A.P. Grosvenor, *J. Phys.: Condens. Matter*, **23**, 465502 (2011).

[2] A. M. Ritzmann, A. B. Munoz-Garcia, J. A. Keith, E. A. Carter, *MRS Comminuciations,* **3**, 161 (2013).

[3] A. Delmastro, D. Mazza, S. Ronchetti, M. Vallino, R. Spinicci, P. Brovetto, M. Salis, *Mater. Sci. Eng. B*, **79**, (2001) 140.

[4] Y.-G. Cho, K.H Choi, Y.-R. Kim, J.-S. Jung, S.-H. Lee, *Bull. Korean Chem. Soc.*, **30**, 1368 (2009).

[5] M.C. Carotta, M.A. Butturi, G. Martinelli, Y. Sadaoka, P. Nunziante, E. Traversa, *Sens. Actuators B.*, **44**, 590 (1997).

[6] J. W. Yoon, M. L. Grilli, E. Di Bartolomeo, R. Polini, E. Traversa, *Sens. Actuators B.,* **76**, 483 (2001).

[7] I. Hole, T. Tybell, J. K. Grepstad, I. Wærnhus, T. Grande, K. Wiik. *Solid-State Electronics,* **47**, 2279 (2003).

[8] N. N. Toan, S. Saukko, V. Lantto, *Physica B.*, **327**, 279 (2003).

[9] Q. Ming, M. D. Nersesyan, A. Wagner, J. Ritchie, J. T. Richardson, D. Luss, A. J. Jacobson, Y. L. Yang, *Solid State Ionics*, **122**, 113 (1999).

[10] T. Arakawa, H. Kurachi, J. Shiokawa, *J. Mater. Sci.*, **20**, 1207 (1985).

[11] S. Thirumalairajan, K. Girija, V. R. Mastelaro, N. Ponpadian, *ACS Appl. Mater. Interfaces*, **6**, 13917 (2014).

[12] K.M. Parida, K.H. Reddy, S. Martha, D.P. Das, N. Biswal, *Int. J. Hyd. Energy*, **35**, 12161 (2010).

[13] H. Su, L. Jing, K. Shi, Ch. Yao, H. Fu, *J. Nanopart. Res.*, **12**, 967 (2010).

[14] Z. Yang, Y. Huang, B. Dong, H. – L. Li, *Mater. Res. Bull.*, **41**, 274 (2006).

[15] W.J. Zheng, R.H. Liu, D.K. Peng, G.Y. Meng, *Mater. Lett.*, **43**, 19 (2000).

[16] S. M. Khetre, H. V. Jadhav, S. R. Bamane, *Rasayan J. Chem.*, **3**,82 (2010).

[17] H. Shen, G. Cheng, A. Wu, J. Xu, J. Zhao, *Phys. Status Solidi A.,* **7**, 1420 (2009).

[18] M. Sivakumar, A. Gedanken, W. Zhong, Y.H. Jiang, Y.W. Du, I. Brukental,D. Bhattacharya, Y. Yeshurun, I. Nowik, *J . Mater. Chem.*, **14**, 764 (2004).

[19] D. Treves, *J. Appl. Phys.*, **36**, 1033 (1965).

[20] J. W. Seo, E. E. Fullerton, F. Nolting, A. Scholl, J. Fompeyrine, J.P. Locquet, *J. Phys.: Condens. Matter,* **20** (2008) 264014.

[21] Inorganic Crystal Structure Database ICSD 371493 Fachinformationszentrum (FIZ) Karlsruhe 2007.

[22] Inorganic Crystal Structure Database ICSD 470067 Fachinformationszentrum (FIZ) Karlsruhe 2007.

[23] H.M. Rietveld, *J. Appl. Cryst.*, **2**, 65 (1969).

[24] R. Delhez, T.H. de Keijser, J.I. Langford, D. Louër, E.J. Mittemeijer and E.J. Sonneveld, Crystal Imperfection Broadening and Peak Shape in the Rietveld Method, in: The Rietveld Method, edited by R.A. Young, Oxford Science, Oxford, United Kingdom, 132 (1993).

[25] L. Lutterotti, S. Matthies and H.-R. Wenk, IUCr: Newsletter of the CPD, **21**, 14 (1999).

[26] S. Geller, E.A. Wood, *Acta Cryst.* **9**, 563 (1956).

[27] M. Romero, R.W. Gómez, V. Marquina, J.L. Pérez-Mazariego, R. Escamilla, *Physica B,* **443** (2014) 90.

[28] M.K. Singh, H.M. Jang, H.C. Gupta, R.S. Katiyar, *J. Raman Spectrosc*. **39**, 842 (2008).

[29] J.E. Spanier, R.D. Robinson, F. Zhang, S.W. Chan, I.P. Herman, *Phys. Rev. B*. **64**, 245407 (2001).

[30] M.A. Islam, Y. Xie, M.D. Scafetta, S.J. May, J.E. Spanier, *J. Phys.: Cond. Matter,* **27**, 155401 (2015).

[31] Y. Du, Z.X. Cheng, X.L. Wang, S.X. Dou, *J. Appl. Phys.,* **107**, 09D908 (2010).

[32] .S. Smirnova, *Physica B* **262**, 247 (1999).

[33] L. Martín-Carrón, A.de Andrés, M.J. Martínez-Lope, M.T. Casais, J.A .Alonso, *Phys. Rev. B* **66**, 174303 (2002).

[34] M.A. Ahmed, N. Okasha, *J. Alloy. Compd.*, **553** (2013) 308.

[35] Shen Hui, Xu Jiayue, and Wu Anhua, J. Rare Earths 28, 416 (2010).